ELSEVIER

Sensors and Actuators A 99 (2002) 125–133

SENSORS AND ACTUATORS A PHYSICAL

www.elsevier.com/locate/sna

Design, fabrication and modeling of solid propellant microrocket-application to micropropulsion

C. Rossi[a,*], S. Orieux[a,b], B. Larangot[a], T. Do Conto[a], D. Estève[a]

[a]*LAAS-CNRS, 7 Ave du Colonel Roche, 31077 Toulouse Cedex 4, France*
[b]*CNES, 18 Ave Edouard Belin, 31501 Toulouse Cedex 4, France*

Abstract

The integration of propellant within a silicon micromachined systems enables the realization of a new class of MEMS devices called microscale rocket. These new devices seem to respond to a real need in the field of high energetic microscale actuation. Their main originality is the use of only one solid propellant loaded in a small tank micromachined in a ceramic or silicon substrate. The structure consists of a sandwich of three micromachined silicon substrates: nozzles, igniters and propellant chambers. The thrust force issued from the combustion of the solid propellant ranges from 1 mN to a few mN. Just by geometrical and dimensional considerations, it is possible to adapt the thrust impulse depending on the application requirements. One identified application of microrockets is space with the realization of microscale thrusters for the control of the attitude or/and the station keeping of very small satellite.

In a first part of the paper, we present the process of fabrication and the assembling of microthrusters as well as the specific equipment developed to load the solid propellant into microcavities. On a second part, we present briefly the modeling tools developed to predict the thruster performances.

Keywords: MEMS; Combustion; Thrust; Solid propellant; Gas flow computation; Silicon

1. Introduction

Micromachining the silicon and ceramic material enables the fabrication of new class of devices. One of them is the microscale rocket. This new type of microdevices has an interest in the growing tendency of miniaturization of every systems [1,4,5]. Indeed, scaling down the dimensions of the system imposes an increase of the energy density stored in the system to produce heat, mechanical force or electrical energy.

Combustion is one simple way to obtain large quantities of energy from a small volume. Typical solid propellant has an energy density of around 5 J/mm^3. Commercial zinc–air batteries have an energy density of just 3 J/mm^3.

Commercial lithium batteries have an energy density of only 0.3 J/mm^3, gold capacitor has an energy density of 9 mJ/mm^3. If the chemical energy contained in the solid propellant can be converted efficiently to useful energy, a microscale combustion device may be very competitive with commercial batteries. But, downscaling the device is unfavorable for efficiency especially when there are moving parts. We can keep in mind 20% for the average efficiency of a microgas turbine of a cubic millimeter. This type of devices face, besides the technological difficulties due to the complexity of the device, an important issue which is the relatively low efficiency of the device mainly due to energetic losses caused by the frictional forces [2,3]. LAAS-CNRS proposes in this paper a solid propellant rocket that avoids some of these problems. The concept of solid propellant rocket is based on the combustion of an energetic propellant stored in a micromachined chamber. It presents the following three main advantages:

1. The frictional forces inherent to moving parts are eliminated.
2. There is not liquid fuel so not leakage possible and the propellant is stable in time.
3. The pressurization of the combustion chamber does not reach the level of microgas turbine that could prevent mechanical failures.

The main limitation of this kind of devices is the lack of restart ability which could be partially compensated by the possibility to fabricate arrays. The most obvious application of these ''thrust generator'' microdevices is the micropropulsion for space application. In this paper, we report the design, the fabrication and the modeling of solid propellant

* Corresponding author. Tel.: +33-561-336301; fax: +33-561-336208.
E-mail address: rossi@laas.fr (C. Rossi).

0924-4247/02/$ – see front matter
PII: S0924-4247(01)00900-1

Nomenclature

a	burn rate coefficient
$A_{c(x)}$	combustion area
A_e	diverging exit area
A_t	throat area
b	burn rate under vacuum
b_{cr}	critical pressure ratio
C	calorific potential under vacuum
C_p	isobaric heat capacity per unit mass
C_v	volumic heat capacity per unit mass
h'	convection coefficient
m	fluid mass in the combustion chamber
m_i	initial fluid mass in the chamber combustion
M_e	Mach number of the diverging exit area
n	burn rate exponent
P	spatial mean pressure in the combustion chamber
P_a	atmospheric pressure
P_e	pressure of the diverging exit area
q_{in}	mass flow rate of the propergol combustion
q_{out}	mass flow rate through throat area
r	gas constant
$S_{(x)}$	heat transfer area of the combustion chamber
T	spatial mean temperature of the gas in the combustion chamber
T_i	initial spatial mean temperature of the fluid in chamber combustion
T_w	combustion chamber wall temperature
$V_{(x)}$	volume of the combustion chamber
x	combustion front ordinate
x_i	initial combustion front ordinate

Greek letters

ε	radiation interchange factor
ϕ_{con}	convection heat transfer
ϕ_{in}	heat transfer by the propellant in the combustion chamber
ϕ_{rad}	radiation heat transfer
γ	isentropic coefficient of the fluid
ρ_p	propellant density
σ	Stefan–Boltzmann constant

microthrusters. One single thruster consists of a stack of the following three parts of silicon:

1. A silicon micromachined igniter: a polysilicon resistor is patterned onto a very thin dielectric membrane. The silicon micromachined igniter section has a double function: heat source that initiates the combustion and throat of the nozzle.
2. A propellant chamber: we use either a low thermal conductive ceramic or a thick silicon substrate. The use of a ceramic substrate may minimize the thermal losses through the system, thus, optimizing the resulting thrust. Furthermore, using ceramic substrates enables us to fabricate thrust chamber length over the millimeter.
3. A diverging part wafer can be added on top of the structure if necessary. For low pressure chamber functioning point, the diverging part does not lead to much better performances at atmospheric pressure. This will be discussed in Section 3.3.Section 2 describes the microfabrication and the assembly of the device. Section 3 presents the model developed to describe the functioning and to predict the performance of our device as well as some modeling results.

2. Microfabrication of the device

The microthruster prototypes we present in this paper have the features and dimensions shown in Fig. 1.

Two devices have been designed and fabricated: one having a throat diameter of 108 μm and a chamber diameter of 850 μm. One having a throat diameter of 250 μm and a chamber diameter of 1 mm. Other dimensions are kept constant.

2.1. Thermal igniter fabrication

A clean 4 in. (1 0 0) oriented silicon wafer is oxidized. Then, we coat the thermal oxide with a layer of silicon rich nitride, the resulting thickness is 0.7 μm. In a third step, a layer of 0.5 μm of polysilicon is deposited by low pressure chemical vapor deposition (LPCVD) at 605 °C and patterned using a reactive ion etching (RIE) plasma of CF_4 and O_2 in order to design the resistor. Then, we realize the electrical pads and electrical supply lines in gold. A square window pattern is opened in the dielectric layer on the wafer back-side by conventional photolithography and RIE etching with CF_4 and O_2 plasma. The silicon is then etched away with anisotropic etchant as KOH. The fabrication yield of the structure with a SiO_2/SiN_x membrane of 0.7 μm thick is very close to 100% [6]. An SEM photo of one microheater array and a SEM photo of one single igniter with the polysilicon resistor are shown, respectively, in Figs. 2 and 3.

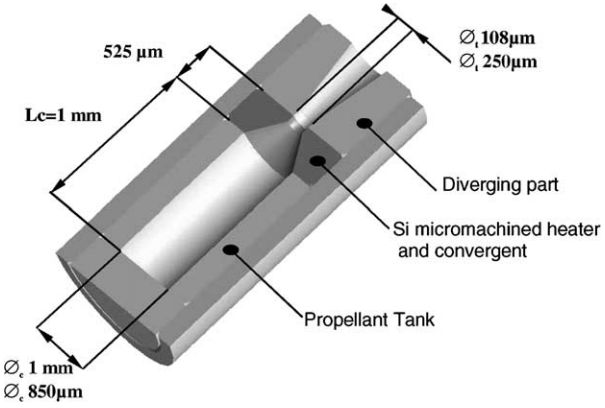

Fig. 1. Schema of the geometrical features of a single microthruster.

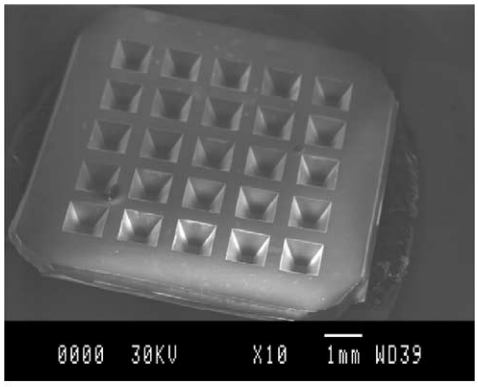

(a)

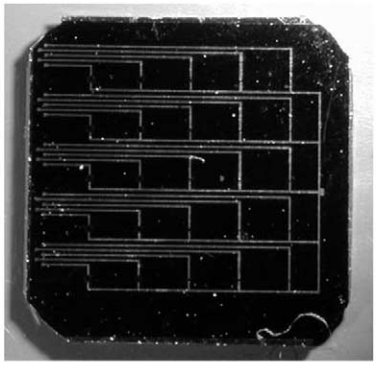

(b)

Fig. 2. (a) SEM photos of the back-side of the igniter wafer; (b) photos of the electrical connections of the igniter wafer.

2.2. Fabrication of the silicon chambers-exploration of ceramic as an alternative material for long chamber

The silicon chambers were realized by deep reactive ion etching (DRIE). In pictures of Fig. 4, we can see a part of propellant chambers array being 9.5 mm × 9.5 mm. It contains a total of 25 square holes of 525 μm thick obtained by DRIE (surface technology systems with inductively coupled plasma). A thick photoresist is used to mask. The etching process is a succession of active cycles (SF_6 gas flow for etching) and passivation cycles (C_4F_8 gas flow). The cavities shown on the photos of Figs. 4 and 5 are 1000 μm × 1000 μm and the spacing is 500 μm. The same process is used to realize 850 μm × 850 μm cavities with a separation wall thickness of 650 μm.

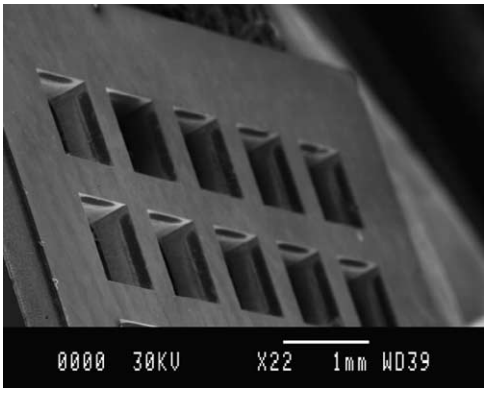

Fig. 4. Photo of one propellant chambers array.

In spite of a high aspect ratio structures (HARS), a comparison can be done between top and backside view of the structure concerning the etching. On top we have perfect patterns and on backside the angles of the square holes are round off. The section view emphasizes this observation. The sidewalls are loosing their verticality during etching time, we approach an etching which is out of the way with 35 μm in width at the bottom.

An alternative material for the fabrication of chamber may be ceramic. Ceramic is very interesting for its good thermal properties by comparison of those of silicon. The thermal conductivity of ceramic materials is between 4 and 10 times less than thermal silicon conductivity depending on the ceramic type. Thermal conductivity can change from 1.46 W/mK (25 °C) for Macor to 35 W/mK (25 °C) for complex ceramics which use a rich composition of alumina (Al_2O_3: 3.89 g/ml in density).The micromachining of the ceramic is possible by laser or ceramic injection micromolding (CIM). Up to now, we have fabricated ceramic chambers of 1 mm of diameter by conventional drilling from MACOR. For further development, LAAS has chosen to

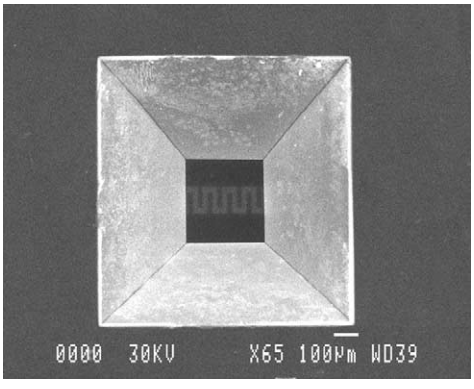

Fig. 3. SEM photo of one single igniter (view from the back-side).

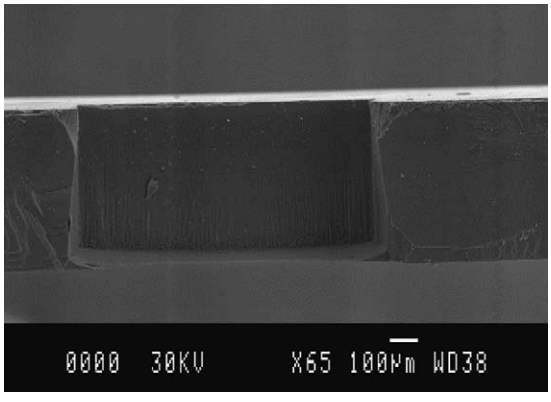

Fig. 5. Cross-section of a propellant chamber made from DRIE.

orient the investigation towards CIM to realize the microchamber.

2.3. Filling and assembling

2.3.1. Fuel characteristics

The propellant is formulated by LACROIX. We work with a composite propellant. The composite propellant is composed of one binder (typically, polybutadiene or glycidyle azide polymer), one oxidizer (typically, NH_4ClO_4) and one fuel (Al, Zr, B, Mg). They present the main advantage to be low vulnerability ammunitions. They have greater specific impulse (Isp) than homogeneous propellant (nitrocellulose and nitroglycerine based propellant). However, metallic particles remain after combustion and composite propellants have a relatively low specific heat value. They have been chosen for microthruster application because they present the ability to be adaptive. Indeed, we can adapt the rheologic, ballistic and kinetic characteristics just by changing the composition and compound rate. In Table 1, we have reported the characteristics of the propellant used at the moment [7].

2.3.2. Propellant injection equipment

Filling the microchamber with viscous material was a key point for the success of such a device. Indeed, cavity free filling of trough or blind holes with a pasty product featuring an important aspect ratio (depth/diameter) is always critical. The air trapped in the blind hole or in the cavity is a limit to the filling and a low viscous product requires a high pressure to be injected in a small aperture without damaging the thin membrane. Previously some vacuum chamber injection machines have been developed and tested. The equipment consists in a vacuum chamber in which the device to be filled and the injection system are installed. The drawbacks of this kind of devices are their cost and their complexity compared to their low efficiency.

The present innovation (patented by NOVATEC SA) brings a new and original solution to the problem of filling holes without the drawbacks of the previous systems and can be fitted on existing stencils printers. The technology is constituted by a specific transfer head which slides across the transfer stencils or directly on top of the substrate to be filled. Compared with existing systems, this innovation shows very high efficiency and reliability level to process in addition to its low equipment cost. The technology is particularly well-suited to plug through or blind holes on a substrate with paste in a collective manner. Fig. 6 shows a schematic view of the process principle and the derivate equipment.

Table 1
Characteristics of the propellant used for the application

Propellant properties	Composite propellant
Composition (main compound)	Oxidizer (NH_4ClO_4), fuel, binder
C (J/g)	2900
$V = aP^n + b$	
a (m/s Pa)	776×10^{-5}
n	0.29
b (m/s)	1×10^{-3}
$\gamma = C_p/C_v$	1.3
ρ (kg/m^3)	1500
C_p	1885

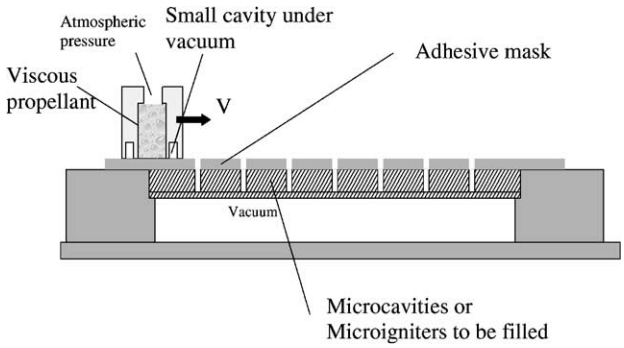

Fig. 6. Schematic view of the process and the equipment set-up to load the propellant inside microcavities.

2.3.3. Final gluing

Each part of the device (the igniter and the reservoir) is first filled with the propellant and then assembled with epoxy mixture glue enabling the entire structure to support combustion pressure inside the combustion chamber. We used EPO TEK H70E glue cured at 60 °C during l5 h. Experimental results demonstrated that the gluing can stand a pressure of 30 bar in the thrust chamber. Tests have been realized at −80 °C, ambient and >100 °C. The microthrusters arrays, thus, fabricated have been tested in ignition. They are on the point to be characterized in order to get experimentally their performances. We will dedicate a full paper on this topic in next months.

3. Performance evaluation and influence of the diverging part

This section is dedicated to the succinct presentation of the modeling tools developed for the following reasons:

1. Firstly, better understand the phenomenon that occurs in microscale gas flow, especially in subsonic regime.
2. Secondly, to set-up a modeling package that could evaluate the functioning and the performance of the microthruster.

The final aim is to have a designing package that could for any given rocket or thruster characteristics, propellant properties and environmental conditions, evaluate the thrust impulse. The model is valid for subsonic and supersonic regime.

3.1. Assumption and model description

3.1.1. Main assumptions

- Pressure and temperature are supposed to be homogeneous in the burning chamber.
- The burning gas is a perfect gas.
- The flow in the diverging and in the throat is assumed isentropic, mono-dimensional and quasi static.
- The variation of the pressure on the burn rate law is neglected.

3.1.2. Model description and computation

The equations are solved using SIMULINK, a toolbox of Matlab [9–12] (Fig. 7). The principle and the equations of the model are expressed in Fig. 7.

3.2. Computational results

In this section, we consider the two chamber-to-throat section ratios: $A_c/A_t = 60$ ($D_t = 108$ μm; $D_c = 850$ μm) and $A_c/A_t = 16$ ($D_t = 250$ μm; $D_c = 1000$ μm). The chamber length is $L_c = 1000$ μm. No diverging part was reported on the microthruster.

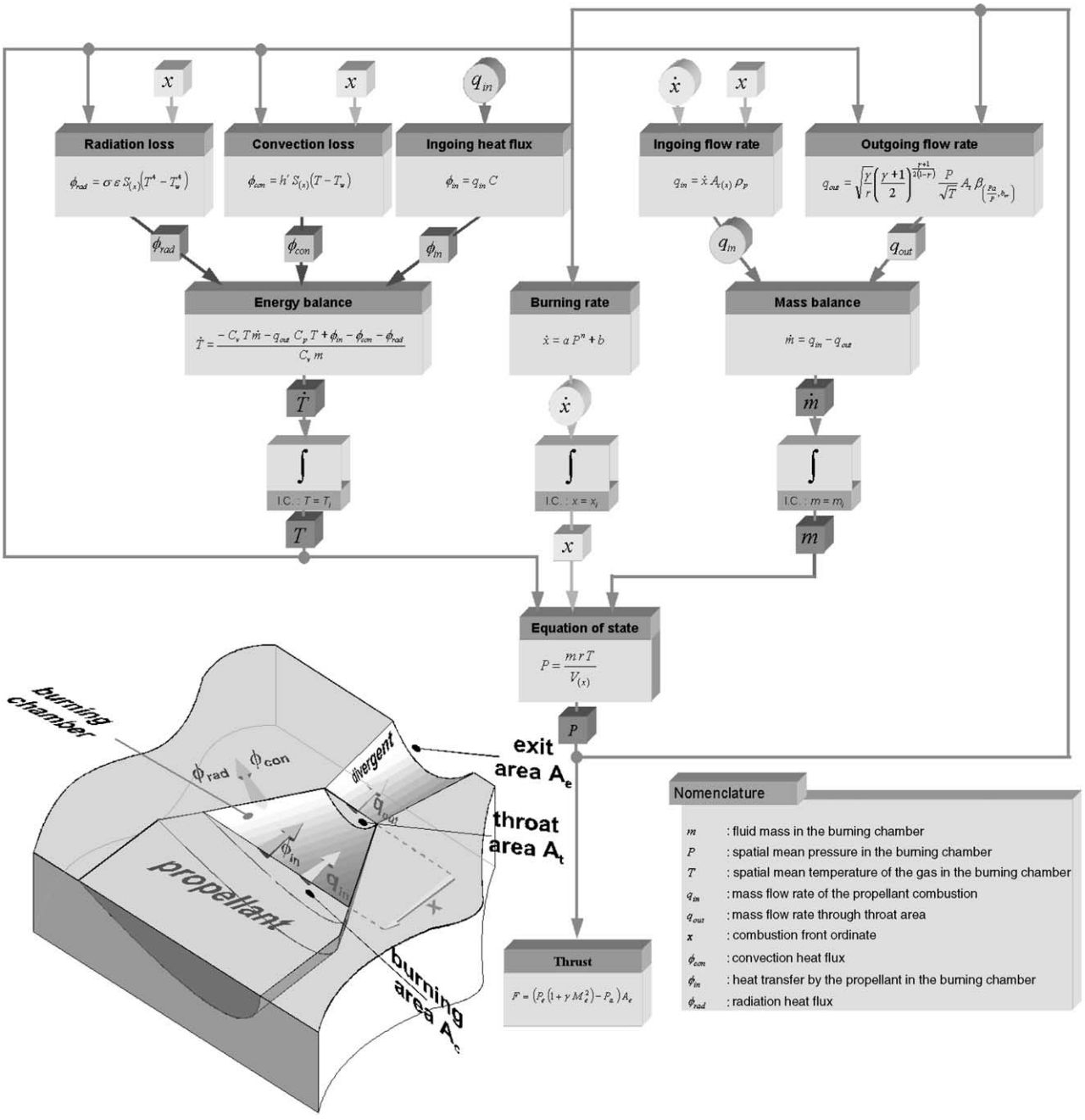

Fig. 7. Principle of the model.

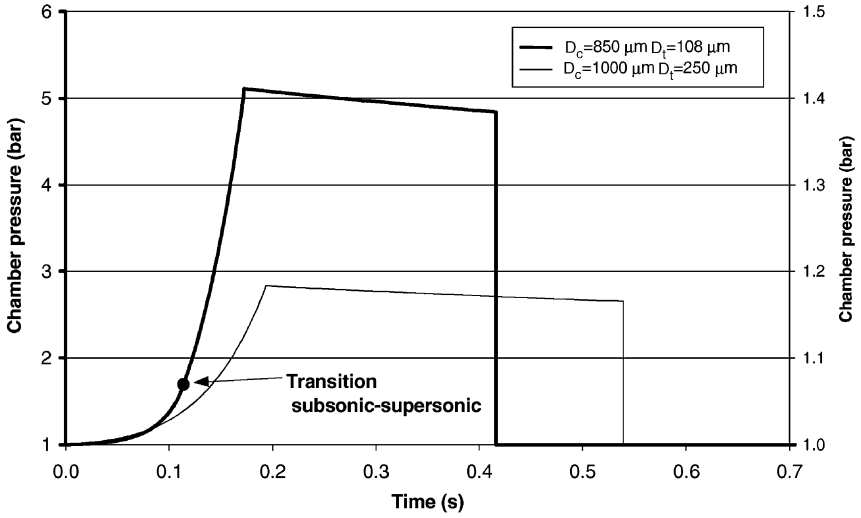

Fig. 8. Chamber pressure as a function of time (at external atmospheric pressure).

3.2.1. External pressure at atmospheric

In the graphs below, we have plotted the chamber pressure variation with the time as well as the variation of the thrust force as a function of the time for both structures.

For structure featuring a chamber-to-throat area ratio of 16, the gas flow remains in a subsonic regime, the critical pressure being equal to 1.73 bar.

For structure featuring a chamber-to-throat ratio of 60, we see in graph (see Fig. 8) that the sonic regime is reached when the pressure in the chamber reaches the critical pressure (1.68 bar). The transition from the subsonic flow to the sonic flow appeared at about 110 ms after the start of the combustion.

In terms of thrust force, the thruster featuring a chamber-to-throat ratio of 60 delivers roughly 4.8 mN over 250 ms. The thruster featuring a chamber-to-throat ratio of 16 delivers <1.5 mN during 350 ms (Fig. 9). This low thrust force is due to the subsonic flow in the throat.

3.2.2. External pressure at vacuum (1 mbar)

For the two microthrusters geometrical features the critical pressure is equal to 1.7 mbar approximately, then the flow is immediately sonic and the pressure for $A_c/A_t = 16$ increases. For $A_c/A_t = 60$, the pressure is approximately the same than atmospheric functioning. Indeed, the sonic flow in the throat stop the external pressure information from coming back to the burning chamber (see Figs. 10 and 11).

In terms of thrust force, *the thruster featuring a chamber-to-throat ratio of 60* delivers roughly 5.8 mN over 250 ms. For $A_c/A_t = 60$, the thrust force is greater when gas flow exhaust at 1 mbar environment than when its exhaust at atmospheric pressure. This is explained by the added force

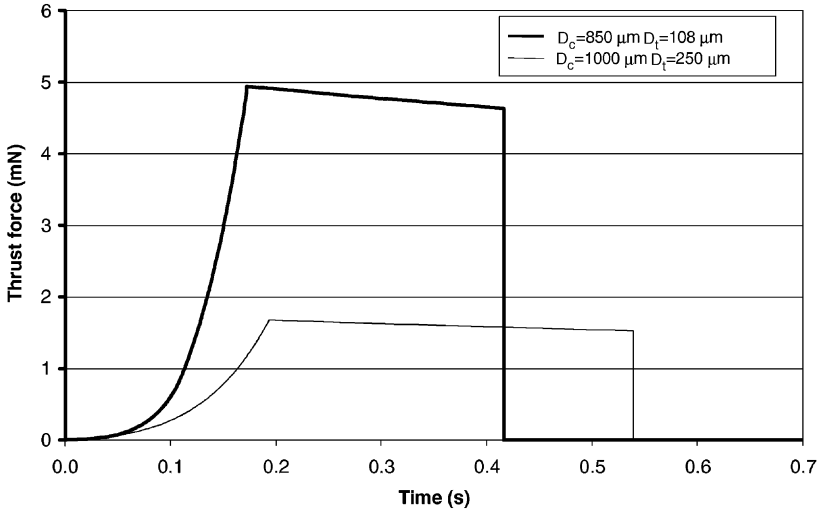

Fig. 9. Thrust force as a function of the time (at external atmospheric pressure).

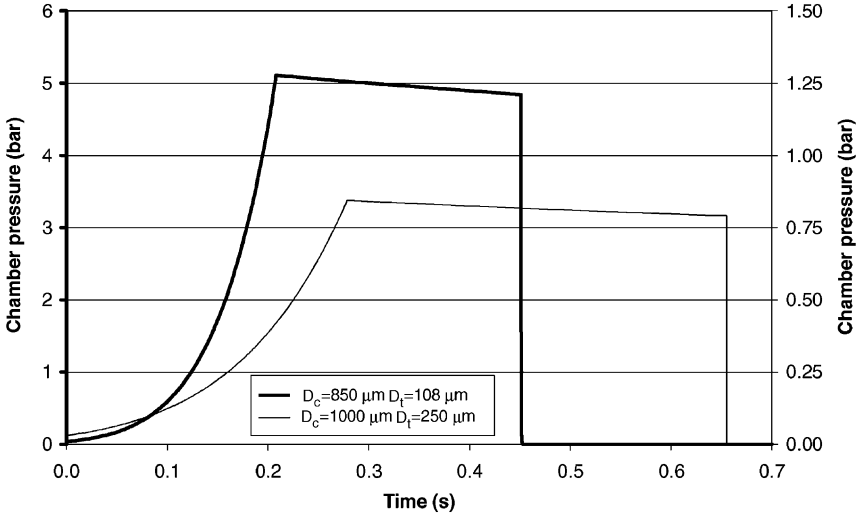

Fig. 10. Chamber pressure as a function of the time (external pressure at vacuum).

due to atmospheric pressure which is equal to 0.9 mN. This force is taken away from the thrust generated by the gas flow.

The *thruster featuring a chamber to-throat ratio of 16* delivers 5 mN during 350 ms. This thrust force increase is due to sonic flow in the throat and to the atmospheric force disappearance.

3.3. Influence of the diverging part on the thrust force

In this section, we discussed the influence of the diverging part on the performances of the microthruster. Usually and in most case found in literature, the nozzle is made of two parts: a converging part that confines the gas, permits the increase of the pressure and permit the sonic flow at the throat. A diverging part that accompanies the flow in the expansion and increases the speed when the flow is supersonic. The typical half angle of the conical diverging part is around 80° [8].

The nozzle is over-expanded when the gas expands to a lower pressure than the external pressure; the exhaust section is too large and the shock wave appears inside the diverging. The nozzle is called under-expanded when the fluid discharged at a pressure higher than the external pressure because the exit area is too small. The nozzle is adapted when the flow exhausts at roughly atmospheric pressure. The optimum nozzle shape is a compromise that depends on the specific application and functioning pressure. That is why we have realized a particular study in order to estimate the influence of the diverging part of the microrocket nozzle and find the optimum configuration for our functioning point.

In the tow graphs below we have plotted the total thrust with the exit-to-throat area ratio (A_e/A_t). The total thrust is obtained by integration of the thrust force in the time. The tow graphs have been plotted for one structure $A_c/A_t = 60$ and for the tow external pressure (atmospheric and vacuum).

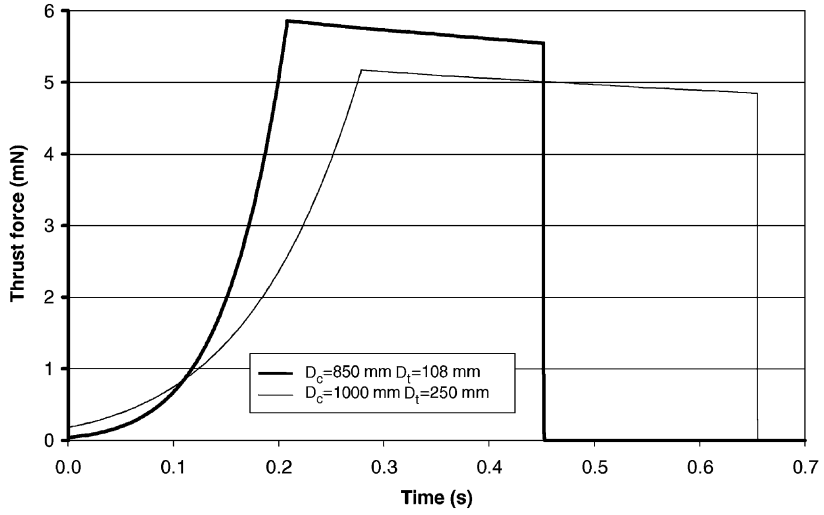

Fig. 11. Thrust force as a function of the time (external pressure at vacuum).

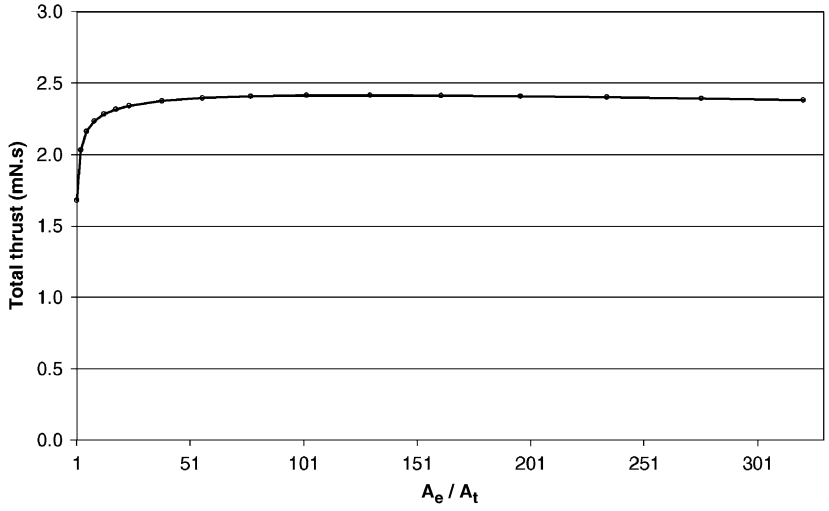

Fig. 12. Total impulse as a function of the area ratio A_e/A_t (external pressure at atmospheric).

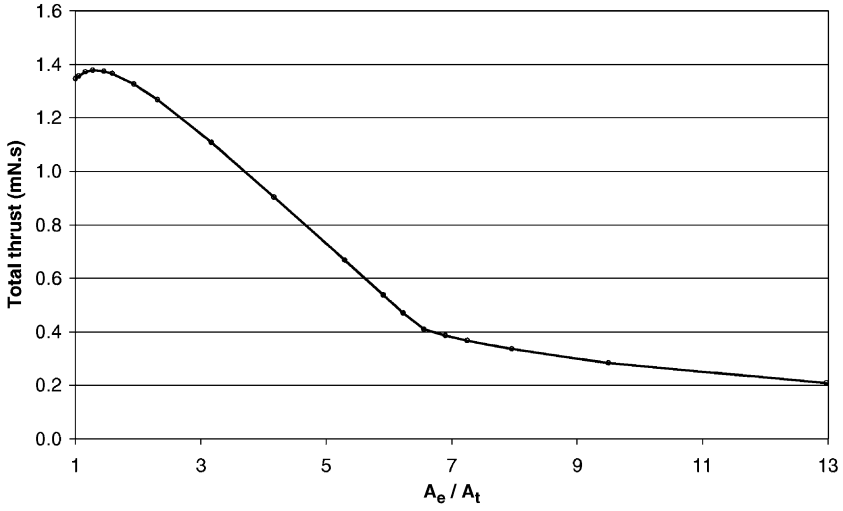

Fig. 13. Total impulse as a function of the area ratio A_e/A_t (external pressure at vacuum).

We see in Fig. 12 that for $A_e/A_t = 1.3$ there is an optimum total thrust that is equal to 1.39 mN s. This optimum gives for a half angle of 8°, a diverging length of 50 μm. Therefore, the total thrust only decrease to 1.35 mN s, for $A_e/A_t = 1$. Then the diverging part is not necessary when the external pressure is equal to atmospheric pressure. This fact is due to the low level of the chamber pressure. The optimum total thrust (equal to 2.4 mN s) is obtained for $A_e/A_t = 130$ and correspond to the case when the external pressure is equal to 1 mbar (see in Fig. 13). The optimum diverging length is around 4000 μm with the a half diverging angle of 8°. These considerations illustrate the great importance of the nozzle investigation.

4. Conclusions and perspectives

Using solid propellant to generate thrust is not very original, but we have seen that it seems to be very novative for small scale thruster and rocket. The solid propellant thrusters we proposed use a fabrication process based on MEMS conventional fabrication methods and the assembly is very simple to proceed. The use of low thermal conductive material for the propellant tank such as ceramic appeared feasible and leads to a minimization of the heat transfer between each thruster. The dependence of the resulting thrust with dimensional and geometrical parameters as well as propellant characteristics, implies that it is possible to fabricate thrusters with a total impulse ranging from 0.1 mN s to 1 N s.

The model we have developed and briefly presented in this paper present the following advantages:

- To be flexible and adaptable easily to different type of thruster and material just by changing the data base, thus, enabling to make optimization.
- To have low calculation time (a few minutes).
- To be correct and usable for subsonic and supersonic regime.

The fabrication of arrays of microthrusters proved the feasibility of the concept. We are characterizing the thrust impulse with a high sensitive and rapid microthrust balance designed and fabricated at LAAS-CNRS. A paper will be fully dedicated to this topic.

Acknowledgements

The work described in this paper was funded by the National Center for Spatial Studies and Development (CNES). We thank the French group Lacroix for its collaboration and expertise in GAP propellant formulation and thruster filling. The technological fabrication, the assembly and operating tests of microthrusters have been realized in the LAAS-CNRS microfabrication Lab.

References

[1] I.A. Waltz, et al., Combustors for microgas turbine engines, ASME J. Fluids Eng. 120 (1998).
[2] A. Mehra, et al., A six-wafer combustion system for a silicon microgas turbine engine, J. Micro Electro Mech. Syst., 9 (4) (2000).
[3] A. Mehra, et al., Development of a Hydrogen Combustor for a Microfabricated Gas Turbine Engine, Solid-State Sensor and Actuator Workshop, USA, 1998.
[4] A.P. London et al., Microfabrication of a high pressure bipropellant rocket engine, Sens. Actuators A 2997 (2001) 1–7.
[5] W. Lindsay, et al., Thrust and electrical power from solid propellant microthrusters, in: Proceedings of 14th IEEE International Conference on Micro Electro Mechanical Systems, Piscataway, USA, 2001.
[6] C. Rossi, P. Temple-Boyer, D. Esteve, Realization and performance of thin SiO_2/SiN_x membrane for microheater applications, Sensors Actuators A 64 (1998) 241–245.
[7] J. Quinchon, J. Tranchant, M. Nicolas, Les Poudres Pour Armes, p. 151.
[8] Rocket Propulsion Elements, 6th Edition, Georges P. Sutton, Wiley, New York, pp. 41–51.
[9] O. Geider, Modélisation et commande d'un actionneur pneumatique à faible coŭt, Thesis, Institute National des Sciences Appliquées de Toulouse, 1997.
[10] P. Carrière, Aérodynamique interne: Tuyères et Jet, course, Ecole Nationale Supérieure de l'Aéronautique et de l'Espace, 1980.
[11] SP-8093, Solid Rocket Motor Internal Insulation, NASA SP-8093, 1976.
[12] K. Ramamurthi, A.E. Muthunayagam, Scale up of propellant burn rate with the size of rocket motor, in: Proceedings of the 13th International Symposium on Space Technology and Science, Tokyo, Japan, 28 June–3 July 1982.